Available online at www.sciencedirect.com
ScienceDirect
Journal of Power Sources 174 (2007) 95–102
JOURNAL OF POWER SOURCES
www.elsevier.com/locate/jpowsour

Fabrication and characterization of micro-tubular cathode-supported SOFC for intermediate temperature operation

Yu Liu [a,*], Shin-Ichi Hashimoto [a], Hanako Nishino [a], Katsuhito Takei [a], Masashi Mori [a], Toshio Suzuki [b], Yoshihiro Funahashi [c]

[a] *Central Research Institute of Electric Power Industry, 2-6-1 Nagasaka, Yokosuka, Kanagawa 240-0196, Japan*
[b] *National Institute of Advanced Industrial Science and Technology, Shimo-shidami, Moriyama-ku, Nagoya, Aichi 463-9560, Japan*
[c] *Fine Ceramics Research Association, 2266-99 Anagahora, Shimo-shidami, Moriyama-ku, Nagoya, Aichi 463-8561, Japan*

Received 11 April 2007; received in revised form 24 August 2007; accepted 28 August 2007
Available online 6 September 2007

Abstract

We report the fabrication and characterization of a micro-tubular cathode-supported cell consisting of a $Ce_{0.9}Gd_{0.1}O_{1.95}$ electrolyte with a Ni–cermet anode on a porous $La_{0.6}Sr_{0.4}Co_{0.2}Fe_{0.8}O_{3-\delta}$/$Ce_{0.9}Gd_{0.1}O_{1.95}$ (60:40 volume) tube (460 μm wall thickness and 2.26 mm diameter). The cells were fabricated by a cost-effective technique involving extrusion molding and slurry coating through a co-firing process. Densification of the ceria film (thickness < 15 μm) was successful by co-firing the laminated electrolyte with the porous cathode at 1200 °C. NiO–$Ce_{0.9}Gd_{0.1}O_{1.95}$ (Ni: $Ce_{0.9}Gd_{0.1}O_{1.95}$ = 50:50 in volume after reduction) was subsequently sintered on the electrolyte at 1100 °C to construct a 10 μm thick, porous and well-adherent anode. The cell having 1.5 cm tube length fed with humidified 30 vol.% H_2–Ar (3% H_2O) yielded the maximum power densities of 0.16, 0.13 and 0.11 W cm^{-2}, at 600, 550 and 500 °C, respectively. It was found that the cell performance is strongly dominated by the tube length, due to a high substrate resistance from the cathode current collections.
© 2007 Elsevier B.V. All rights reserved.

Keywords: Solid oxide fuel cells; Cathode-supported SOFC; $La_{0.6}Sr_{0.4}Co_{0.2}Fe_{0.8}O_{3-\delta}$; Gadolinium-doped ceria oxide; Co-firing

1. Introduction

Ohmic loss of the electrolyte and cathodic polarization resistance are two important issues that hinder solid oxide fuel cell (SOFC) lowering operation temperature from the traditional 1000 °C to an intermediate range of 500–800 °C. The ohmic loss can be decreased by the reduction of thickness of the conventional yttria stabilized zirconia (YSZ) electrolyte and/or the use of materials with faster ionic transport over YSZ, such as doped ceria [1], scandia stabilized zirconia [2] and doped lanthanum gallate [3]. To decrease the cathodic polarization, various promising alternatives, including of perovskite-type oxides, *i.e.*, $La_{1-x}Sr_xCo_yFe_{1-y}O_{3-\delta}$ [4], $Ba_xSr_{1-x}Co_{1-y}Fe_yO_{3-\delta}$ [5] and K_2NiF_4-type oxides, *i.e.*, $La_2NiO_{4-\delta}$ [6] have been explored to the conventional $La_{1-x}Sr_xMnO_{3-\delta}$.

As one of the usual cell forms, tubular geometry has attracted much interesting due to better thermo-cycling behavior and higher sealing feasibility over planar design [7]. Once the cell diameter gets smaller, *i.e.*, in the millimeter or sub-millimeter range, several potential advantages further appear [8,9]. First, due to the substantial increase in reactive area per unit volume of a stack, it can possibly achieve a higher volumetric power density. Secondary, reduction in wall thickness of tube significantly alleviates the difficult for mass transportation (gas diffusion activity), which is a major barrier to the cell performance. The micro-tubular designs that possess a rapid start-up characteristic due to high-thermal shock resistance are promising for cogeneration and transportation application. Many recent efforts for the micro-tubular cells that can operate at intermediate temperature are mainly based on the anode-supported thin film because of its easy fabrication [10,11]. These cells can be capable of yielding high-power densities below 650 °C due to a significantly reduced ohmic resistance of the thin-electrolyte in association with the selection of suitable materials and the development of advanced fabrication techniques. For

* Corresponding author. Tel.: +81 46 856 2121; fax: +81 46 856 5571.
E-mail address: yu@criepi.denken.or.jp (Y. Liu).

0378-7753/$ – see front matter © 2007 Elsevier B.V. All rights reserved.
doi:10.1016/j.jpowsour.2007.08.101

Table 1
Powders characteristics for the cell components

	Average particle size (D_{50}) (μm)	Specific surface area ($m^2\ g^{-1}$)	Theoretical density ($g\ cm^3$)	Preparations	As cell components
$La_{0.6}Sr_{0.4}Co_{0.2}Fe_{0.8}O_{3-\delta}$	0.50	9	6.330	Citrate method	Cathode
$Ce_{0.9}Gd_{0.1}O_{1.95}$	0.22	30	7.214	Newly devised low-temperature process in coprecipitation [15]	Electrolyte
	0.66	39	7.227	Citrate method	Cathode
NiO–$Ce_{0.9}Gd_{0.1}O_{1.95}$ (Ni:$Ce_{0.9}Gd_{0.1}O_{1.95}$: 50:50 in volume after reduction)	0.40	14	7.005	Citrate method	Anode

instance, Suzuki et al. fabricated the cell consisting of a $La_{0.6}Sr_{0.4}Co_{0.2}Fe_{0.8}O_{3-\delta}$ cathode with a thin $Ce_{0.9}Gd_{0.1}O_{1.95}$ electrolyte on a Ni–cermet support tube (diameter: 1.6 mm) using the cost-effective wet co-firing process, and demonstrated a high-power density of $1.0\ W\ cm^{-2}$ at 570 °C with H_2 fuel [11].

In contrast, there is few work published to data for the cathode-supported thin film under micro-tubular configuration, although it delivers several desired feasibilities, *i.e.*, allowing the using of metal (Ni) for electrical connection for cells, and relatively high-mechanical stress during thermal or redox cycling. This can be highly attributed to the fabrication difficulties of a dense thin electrolyte on a porous cathode. For instance, densification of thin electrolyte in the well-known wet-ceramic co-firing technique is generally achieved by co-sintering the laminated electrolyte with the support electrode at a relatively high temperature, *i.e.*, 1400 °C for a typical Ni–cermet anode-supported cell [10,11]. This represents a high risk to introduce several severe issues for the cathode-supported cell including of (1) chemical reactions between cathode and electrolyte, (2) excessive coarsening of cathode particles with loss of triple phase boundaries (TPB) for oxygen reduction reaction and (3) dense electrode structure with little porosity, which significantly raises the impedance to gas transport [12–14]. The development of the pervious cathode-supported thin film structure in Siemens–Westinghouse is based on electrochemical vapor deposition (EVD) processes to avoid high-sintering temperature during densification of the electrolyte [7].

In pervious report, we have fabricated a small planar cell that consists of a thin, supported electrolyte with a thin Ni–cermet on a porous cathode via a cost-effective wet ceramic co-firing process [12]. The promising combination of $La_{0.6}Sr_{0.4}Co_{0.2}Fe_{0.8}O_{3-\delta}$ and $Ce_{0.9}Gd_{0.1}O_{1.95}$ was used as cathode and electrolyte. Densification of the $Ce_{0.9}Gd_{0.1}O_{1.95}$ membrane was successful on the porous substrate at 1200 °C while the shrinkage between cathode and electrolyte was highly tailored to avoid any deformation and crack in either layer during co-sintering. Regarding the advantages of both micro-tubular and cathode-supported configurations, this work thus applied the above technology to fabricate such a cell, with a specific interest to use the $La_{0.6}Sr_{0.4}Co_{0.2}Fe_{0.8}O_{3-\delta}$/$Ce_{0.9}Gd_{0.1}O_{1.95}$ couple for intermediate temperature operation.

2. Experimental

2.1. Sintering behavior, thermal expansion and electrical conductivity measurements

The preparations of the powders for cell components can be referred to pervious report [12]. Powders characteristics were summarized in Table 1. To investigate the sintering characteristics, the as-prepared powders were pressed to discs in 20 mm diameter and 2–3 mm thickness by uniaxial dry pressing at 200 MPa. This was followed by sintering at selected temperatures over the 600–1200 °C range with a heating rate of $3.3\ °C\ min^{-1}$. The dimension and weight of the unfired and sintered discs were measured to determine the bulk density and the shrinkage. Theoretical density was calculated using the theoretical value determined from the experimental lattice parameters and unit formula based on X-ray diffraction (Mac-Science M18XHF, Japan). The relative density was derived from a ratio of bulk density to theoretical. The shrinkage of the discs was determined as $100 \times (d_2 - d_1)/d_1$, where d_1 and d_2 are initial and final diameter, respectively. Microstructure of the sintered samples was recorded by scanning electron microscopy (SEM, Hitachi, S-3500H, Japan). Linear thermal expansion was measured in air and H_2 from 50 to 650 °C using Mac Science 5000S system by sintered rectangular shapes of 20 mm × 5 mm × 5 mm. A heating/cooling rate was $2\ °C\ min^{-1}$, with a 5 min annealing time at maximum temperature. Decomposition behavior of binder and pore formers was measured by thermogravimetric (TG) analysis using Mac Science 5000S system at the temperature range of 30–1000 °C with a heating rate of $2\ °C\ min^{-1}$ in air. Electrical conductivity was measured by the four-terminal method using a sintered rectangular bar. The potential and current leads were contacted by applying platinum paste and fixing platinum.

2.2. Fabrications of the micro-tubular cathode-supported cells

$La_{0.6}Sr_{0.4}Co_{0.2}Fe_{0.8}O_{3-\delta}$ (LSCF)/$Ce_{0.9}Gd_{0.1}O_{1.95}$ (GDC) tubes were extruded from a plastic mass through a die forming a 3 mm outside diameter. The mass was created by mixing the as-prepared LSCF and GDC powders under a desired volumet-

ric ratio (LSCF:GDC = 60:40 volume) in water for 1–2 h in the presence of ethyl cellulose as binder and polymethyl methacrylate (PMMA) beads as pore-former. A vacuum was applied to the mixing chamber for 10–30 min to remove air from the mass. The mass was left to age over night and then extruded using a ram extruder (Ishikawa-Toki Tekko-sho Co. Ltd., Japan) with an in-house designed die. After drying, the tubes were cut to a desirable length and dip-coated in the GDC slurry, which was prepared by ball-milling the GDC powder, organic ingredients, such as binder, dispersant and solvents for 24 h. These were co-fired at 1200 °C for 10 h with a heating and cooling rate of 2.9 and 5 °C min^{-1}, respectively. Cathode tubes with the dense electrolyte were further dip-coated in an anode slurry containing NiO–GDC (Ni:GDC = 50:50 in volume after reduction) powders with organic ingredients and graphite as pore formers. These were finally fired at 1100 °C for 1 h. The heating rate for the anode formation was 2.9 °C min^{-1}.

2.3. Electrochemical measurements

The electrochemical performance of the single micro-tubular cathode-supported cell was measured under the apparatus shown in Fig. 1a. The current collection was done with a mode shown in Fig. 1b where Pt meshes used as current collectors were covered to the anode section and Pt wires were well wound at two terminals of the tube as cathode current collectors. These were fixed with Ag paste and further heated to 800 °C for 5 h in air. About 30 vol.% H_2–Ar (saturated with H_2O vapor at 20 °C) and air gases were flowed through the anode and cathode in a counter-flow arrangement with a flow rate of 100 mL min^{-1}. The electrochemical measurement was carried out in the temperature range from 500 to 600 °C. Gas sealing was ensured by using the thermosetting sealants such as Aron ceramic C and C.C (Toagosei Co. Ltd.). No gas leakage in the electrochemical measurements was confirmed using bubble-type gas flow meter. Power generation was measured using a current pulse generator (Nikkokeisoku, NCPG-105S, Japan) as a load, with an electrometer (Hokuto-denko, HC-104, Japan) to record the terminals voltages. During the measurement, the effective anode reactive areas for the cells with tube length of 1.5 and 2 cm were 0.07 and 0.22 cm^2, respectively. Current densities were calculated based on the anode areas. The impedance analysis was carried out using a Solartron 1260 frequency response analyzer with a 1296 interface. Microstructures of the micro-tubular cells were recorded with scanning electron microscopy (SEM) and energy dispersive X-ray analysis (EDX) (Hitachi, S-3500H, Japan).

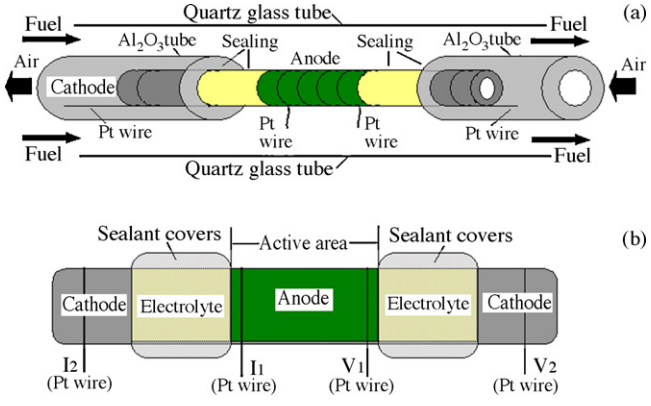

Fig. 1. (a) Schema of the experimental apparatus for the single micro-tubular cathode-supported cell measurement; (b) the enlarged view at the cross section of the sealant cover and current collection through the cell, I_1, I_2: current collect terminals, and V_1, V_2: voltage detect terminals.

3. Results and discussion

3.1. Fabrication of the micro-tubular cathode-supported cells

The tube is required to provide a high mechanical strength after extrusion and further have a high porosity >40% after sintering due to a mass transportation limitation [7]. This can be achieved by introducing the suitable binder and pore former without altering shrinkage characteristics of the ceramic body. Decomposition behaviors of ethyl cellulose (a common binder for ceramics extrusion [16]), and pore formers including PMMA beads and carbon beads were investigated. It was shown in Fig. 2 that the decompose temperatures, *i.e.*, ≤400 °C for PMMA and ≤550 °C for ethyl cellulose, are relatively lower than the shrink beginning temperature of *ca.* 700 °C for the substrate. This avoids the influence on the shrinkage behavior of the cathode. In contrast, the carbon beads, which have higher decompose temperatures (800–1000 °C), highly retard the shrinkage of the ceramic body.

The effect of changing the amount of ethyl cellulose and PMMA beads and identity on both the shrinkage and relative density of the ceramic body was further shown in Fig. 3. As expected, relative density, which potentially indicated a residual porosity, decreased with increasing polymer amounts while maintaining necessary linear shrinkage. However, a higher content of ethyl cellulose (*i.e.*, >5 wt.% *vs.* ceramic) was found to be obviously harmful to the morphology of ceramic substrate, as shown in Fig. 4, postulated as being caused by the gel-aggregation of ethyl cellulose during mixing. Suitable type ethyl cellulose with a relatively high viscosity was thus selected

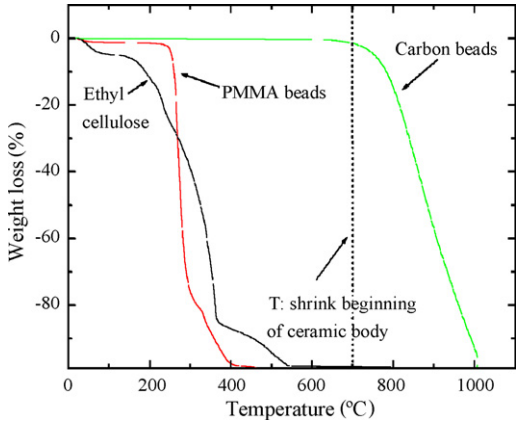

Fig. 2. TG curve of ethyl cellulose, PMMA beads, and carbon beads as a function of temperature in air.

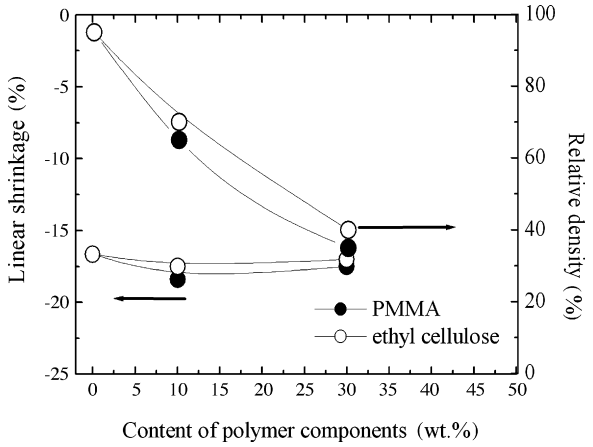

Fig. 3. Linear shrinkage and relative density of the cathode substrates sintered at 1200 °C for 0 h as a function of the contents of PMMA and ethyl cellulose.

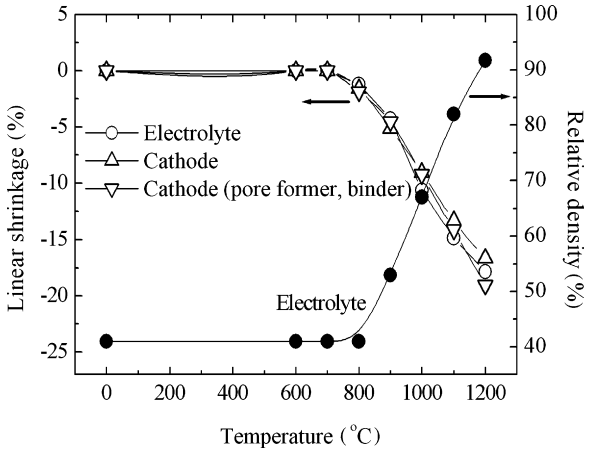

Fig. 5. Temperature change as a function upon the linear shrinkage of the electrolyte and the cathode (without and with binder and pore formers); relative density of GDC was plotted as a function of temperature.

to ensure a high-mechanical strength with a possibly low content of 5 wt.% [16].

Fig. 5 shows linear shrinkage of the cathode (without and with pore former and binder) compared with the GDC electrolyte; relative density of the GDC powder was plotted as a function of temperature. Due to the high surface solid-state diffusion of the nano-sized GDC (specific surface area: 30 $m^2\ g^{-1}$), high density ≥92% of theoretical for the electrolyte was reached at 1200 °C. Increase in the holding time to 10 h further gave a rise to the densification with a relative density >98%. According to a detailed investigation that has been performed previously [12], the cathode contains 40 vol.% (*ca.* 43% by weight) nano-GDC with specific surface area of 39 $m^2\ g^{-1}$ besides the LSCF. By this, the shrinkage of the cathode can match well with that of the electrolyte in 800–1200 °C range. Fine scale powders of GDC are further expected to improve the TPB area leading to a low-cathodic polarization. For such composites, 30–40% by weight of gadolinium-doped ceria was reported as being optimum for an improved electrochemical performance [17]. It can be seen in Fig. 5 that 20 wt.% of PMMA plus 5 wt.% ethyl cellulose (*vs.* ceramic) can be introduced without altering shrinkage characteristics for the LSCF–GDC. The relatively lower decompose temperatures of ethyl cellulose and PMMA appear to be the consequence. Furthermore, the formed pores are thermodynamically stable during sintering since the pore size (*ca.* 5 μm) is much larger than the grains size (*ca.* 1 μm) of the ceramic substrate with larger number of surrounding grains (as confirmed by SEM) [18]. Optimum in the sintering properties and sintered microstructure makes it possible to laminate the dense GDC thin-film to be compatible with the porous substrate allowing co-firing at 1200 °C without introducing undue stress or cracks in either layer.

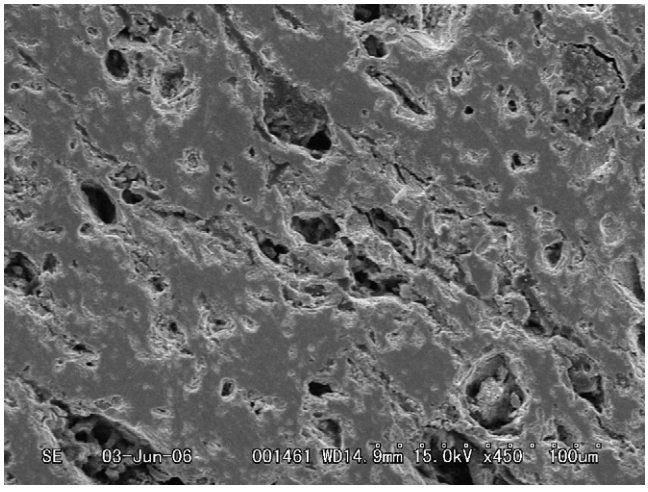

Fig. 4. SEM micrograph of the cross section of the LSCF–GDC (60:40 volume) substrate containing 12 wt.% ethyl cellulose after sintered at 1200 °C for 10 h.

After drying, the as-extruded cathode tube shows a high-mechanical strength that can allow its length being desirably long, as shown in Fig. 6a-1. The shrinkage after sintering at 1200 °C for 10 h was 24.7%, which is in good agreement with the values in Fig. 5. Fig. 6a-2 shows the photograph of a typical cell whose wall thickness and outer diameter were 0.46 and 2.26 mm, respectively (see Fig. 6b). Microstructure of the cathode and anode layers near the electrolyte where most of the electrochemical reaction occurs was further shown in Fig. 6c, in which the cathode possesses uniform and spherical pores (*ca.* 5 μm; porosity: approximately 50%) suggesting that the PMMA beads were homogeneously distributed throughout the substrate prior to sintering. The two oxides (LSCF and GDC) were not separated completely from each other, but were agglomerated in a mixture. Fine Ni–cermet powders used in this study allowed lower sintering temperatures (<1200 °C) to avoid the destruction of the microstructure of the as-established cathode in the subsequent anode formation. The process allows to achieve a good adhesion at both the anode–electrolyte and the electrolyte–cathode interfaces. The dense GDC film showed thickness of *ca.* 12–15 μm and did not exhibit cracks or pinholes, that were further confirmed by SEM observations on the electrolyte surface, as shown in Fig. 6d, where the grain size was approximately 0.5–1.5 μm.

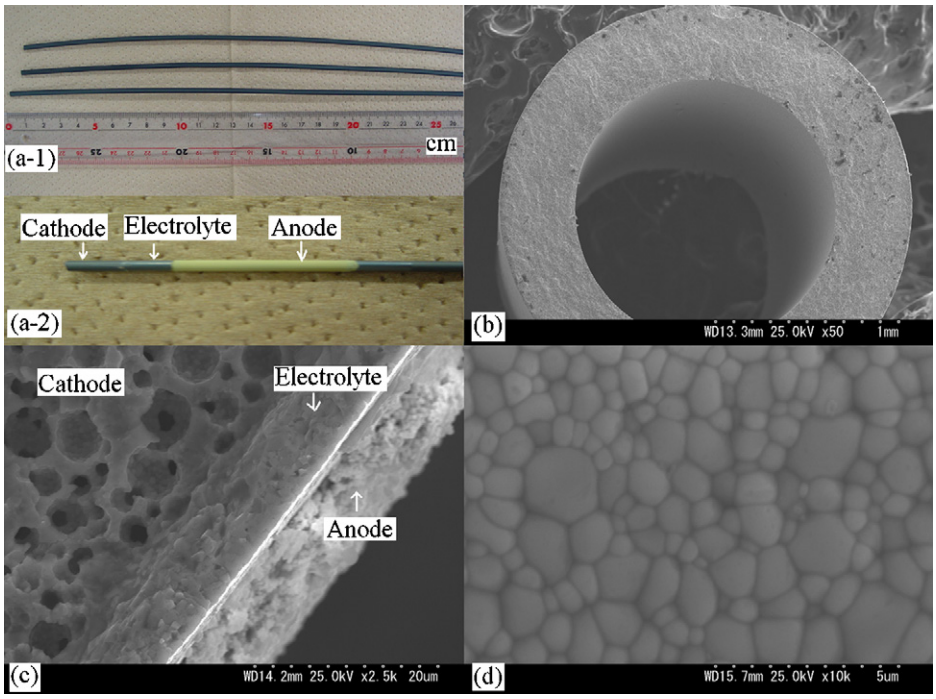

Fig. 6. Photographs of (a-1) cathode tubes after extrusion, and (a-2) a typical cell; SEM micrographs of (b) cross section of the tube, (c) cross section at the cathode/electrolyte/anode interface and (d) surface of the dense electrolyte.

3.2. Thermal expansions of cell components

Matching in the thermal expansions of the cell components is essential to maintain a high reliance under operation conditions. Fig. 7 shows the linear thermal expansions of LSCF–GDC, GDC and NiO–GDC as a function of temperature. The cell components showed coinciding thermal expansions with <0.2% difference at ≤600 °C in air. The change in atmosphere to a reducing environment for both the anode and electrolytes leads to an obvious volume expansion, which in turn results in mechanical stresses. At 650 °C, the thermal expansion coefficient (TEC) of the LSCF–GDC cathode was 11.5 to $12.0 \times 10^{-6}\,°C^{-1}$ (air), as compared to $14.1 \times 10^{-6}\,°C^{-1}$ for the dense GDC (H_2), and further $16.0 \times 10^{-6}\,°C^{-1}$ for the Ni–cermet (H_2). The reduction of ceria appears to be the major consequence in addition to the high thermal expansions of the metallic Ni. However, no crack and destruction was observed for the cells during the repeated thermal cycles under the operation conditions. This can be partly benefited from the micro-tubular geometry [8–10]. In addition, the cathode-supported cell with a thin anode layer that is not dominating the mechanical integrity of the GDC membrane is promising and efficient to lower the influence associated with the bulk volume change resulting from the thermal expansions [19]. It is thus expected that this type cell can be operated without introducing the mechanical instability typical of the anode, leading to a high reliability.

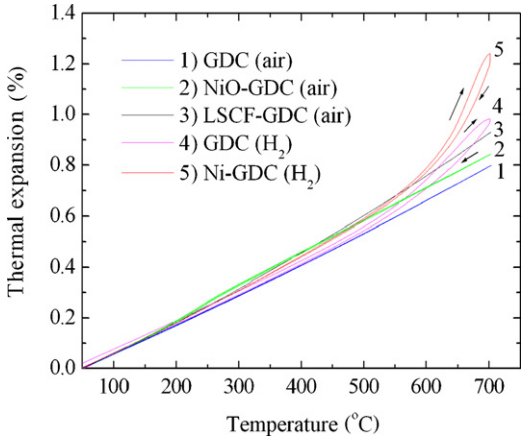

Fig. 7. Thermal expansions of the cell components of cathode (LSCF–GDC), electrolyte (GDC) and Ni–cermet anode, in air and H_2.

3.3. Electrical conductivity of the porous tube

Electrical conductivity of the porous substrate has been proven to be one of the key performance-limiting factors for the cathode-supported cells [7,20]. Fig. 8 shows electrical conductivity of the porous tube, while influence from the porosity and GDC contents was clarified for comparison. The dense LSCF shows a fairly high conductivity of *ca.* 310 S cm^{-1} in 500–600 °C range. The conductivity of the p-type conductor (LSCF) gradually increases up to 600 °C and then slightly decreases. This decrease in the conductivity is attributed to the increase in oxygen non-stoichiometry arising from a decrease in the concentration of p-type charge carriers at high temperatures [4]. The porous LSCF had an electrical conductivity (145 S cm^{-1}) two and a half times smaller than the dense one, and this decrease could be explained by the difference in the charge carries (electron) transport characteristics in a dense or porous body, which is strongly influenced by the microstruc-

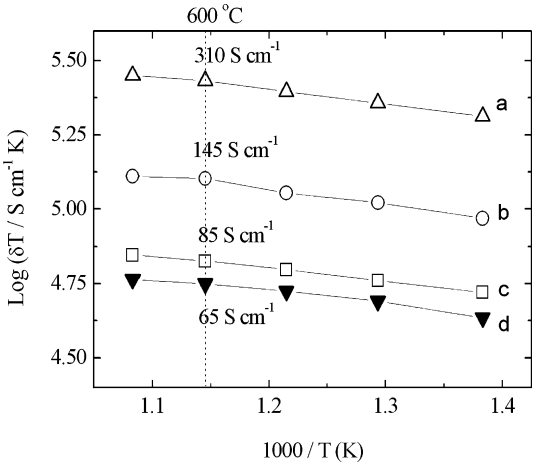

Fig. 8. Arrhenius plot of the conductivity of (a) LSCF (porosity < 5%), (b) LSCF (porosity: 50%), (c) LSCF-GDC (60:40 volume, porosity: 50%) and (d) as-prepared cathode tube (2.26 mm diameter and 460 μm wall thickness). The values at 600 °C were highlighted.

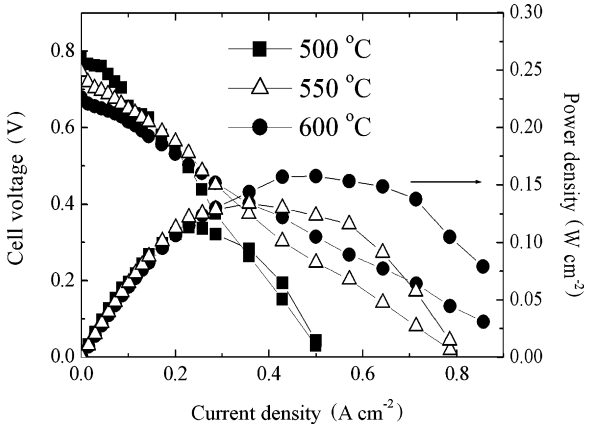

Fig. 9. Current–voltage and power density characteristics of the cell.

ture and sintering condition. The electrical conductivity further decreased with adding of the GDC. The present LSCF–GDC tube has a conductivity of 65 S cm^{-1} (600 °C). It is suggested that the porous cathode can provide relatively high conductivity while maintaining high porosity (50%). Further optimum on the microstructure and dimension that are variably affecting the electrical conductivity remains to be done.

3.4. Electrochemical properties

Since a current-collection model (Fig. 1b), in which the cathode current collections are taken from the terminal of the tube, is introduced for the electrochemical measurement for the single cell [10], the cathode tubes thus become the current collectors, which in turn raise an obstacle to the cell performance since the substrate resistance is linearly dependent on the tube length.

Under such a measurement limitation, the cell still demonstrated a relatively high-power density. Fig. 9 shows the power and *j–V* performance for a typical cell with 1.5 cm tube at 600, 550 and 500 °C. The cell polarization curves were almost linear in all current density range. The maximum power densities reached at 0.16, 0.13 and 0.11 W cm^{-2}, at 600, 550 and 500 °C, respectively. The open circuit voltage (OCV) obtained here is relatively low due to the use of ceria-based electrolyte.

The OCV drops could be partly attributed to the interfacial reaction associated with the elemental diffusion from LSCF to GDC that causes microstructure degradation of the electrolyte during co-sintering of the electrolyte and cathode. Fig. 10 shows cross-sectional SEM micrograph and elemental distribution of the co-fired cell. Small trace of transition metal of Co and Fe (<2 mol.%, as confirmed by energy dispersive X-ray analysis, EDX) was found in the electrolyte layer. Small additions (<2 mol.%) of transition metal oxides into the doped ceria have been reported to considerably favor the densification [21]. It can be explained by a formation of an amorphous transition metal rich grain boundary film that facilitates the densification via liquid phase with a minimum of grain growth. The minor dopant additions have no essential effect on total and ionic conductivity, but considerably increase the p-type electronic transport

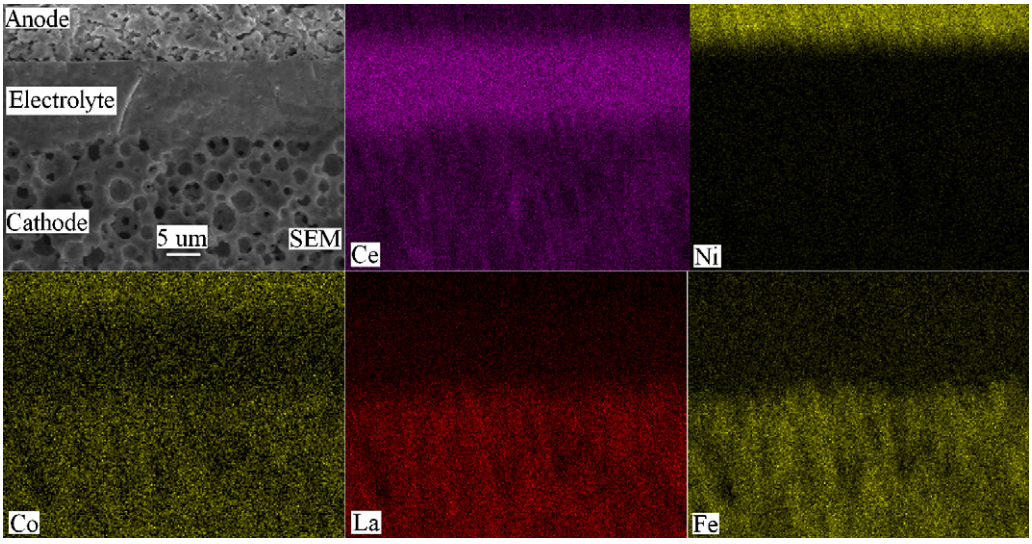

Fig. 10. Cross-section of the co-fired cell: SEM micrograph and elemental mapping distribution of Ce, Ni, Co, La and Fe.

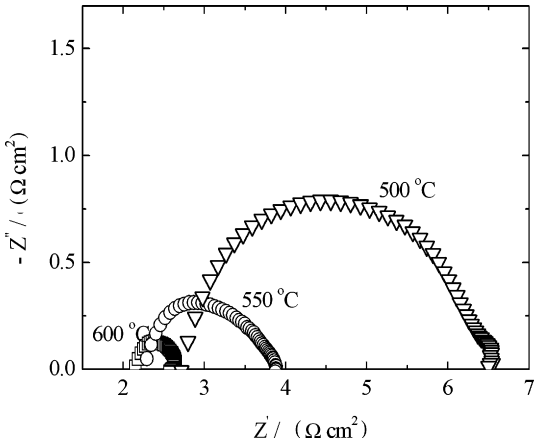

Fig. 11. Impedance spectra for the cell measured at different temperatures.

[21]. Further investigation regarding how such effect influences the thin electrolyte membrane associated with the cell design and electrode microstructure, and optimum in the co-firing conditions remains to be done.

AC impedance spectroscopy was carried out to further reveal which parts of the cell contributed most to the performance. The results obtained under open circuit conditions at 600, 550 and 500 °C are shown in Fig. 11, in which a large impressed arc appeared indicating the charge transfer at the electrode and electrode/electrolyte interface and the mass transportation processes.

Fig. 12 shows the area specific resistances (ASRs) contributed from different parts for the cell as a function of temperature. For the comparison, the ASRs of the GDC electrolyte with a 15 μm thickness were given based on the conductivities of GDC from the literature (0.095, 0.017 and 0.0253 S cm^{-1} at 500, 550 and 600 °C) [1]. At 500, 550, 600 °C, the ASRs of ohmic type did not vary much with the change of temperature, and were 2.73, 2.24 and 2.1 Ω cm^2, which are almost 15 times higher than the ohmic resistances based on the 15 μm thick GDC. This large deviation confirms the influence from the current collection loss for the cathode. The ASRs of non-ohmic resistances (total) at

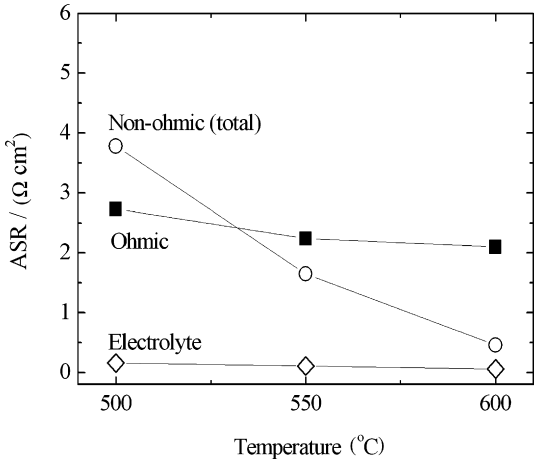

Fig. 12. Area specific resistance (ASR) of the different resistances for the cell in comparison with the resistance of thin GDC electrolyte.

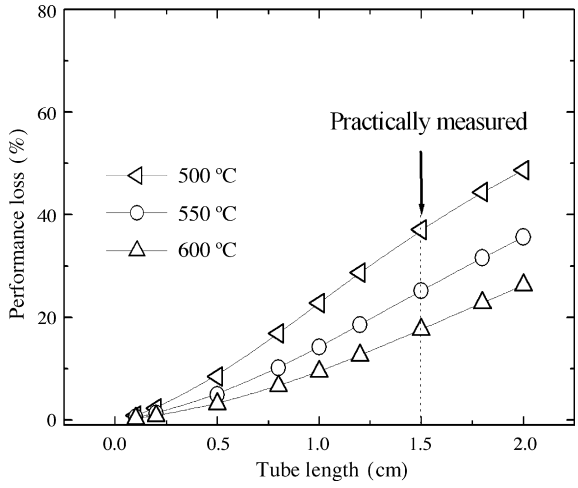

Fig. 13. Calculated performance loss as a function of tube length.

500, 550 and 600 °C were 3.78, 1.65 and 0.46 Ω cm^2. The non-ohmic resistances that indicates the polarization losses including of two general categories of concentration polarization due to resistance to gas transport, and activation polarization due to limitations in the charge-transfer process, obviously decreased as the temperature increased, indicating that the electrochemical reaction kinetics are mainly dominated by the cathode side [20].

3.5. Influence of tube length on cell performance

Using the values of the tube conductivity given in Fig. 8 and power performance in Fig. 9, we can detect the influence of the tube length on the cell performance loss under the present current collection. The calculated result of the performance loss as a function of the tube length was shown in Fig. 13. The detailed calculation can be referred to pervious publication by Suzuki et al. [22]. The performance loss increased significantly as increasing the tube length due to the increased cathode resistance as a current collector. The practically measured cell with 1.5 cm tube was highlighted. At 500, 550 and 600 °C, its performance loss reached at 37, 26 and 17%, which are obviously higher than those of the anode-supported cell under a similar composition and configuration of LSCF–GDC (cathode) and GDC (electrolyte) on Ni–GDC (anode tube) [11,22].

Fig. 14 further compared the maximum powder densities practically measured for the cells with different tube length as 1.5 and 2 cm. The decrease in maximum power density was noticeable with increasing the tube length, *i.e.*, 0.16, 0.13 and 0.11 W cm^{-2} for the 1.5 cm cell, *versus* 0.090, 0.049 and 0.030 W cm^{-2} for the 2 cm one, at 600, 550 and 500 °C. The measured values for the 2 cm tube have a deviation as compared with the calculated ones (0.11, 0.08 and 0.06 W cm^{-2}) according to Fig. 13. It could be attributed to the influences from other factors, such as gas diffusion activity through the porous tube.

The results clearly suggest that the cell performance is strongly limited by the tube length due to the present current collection for the cathode. Therefore, an optimum in the cathode current collection might be very effective to the single cell performance. For instance, this can be realized by impregnating

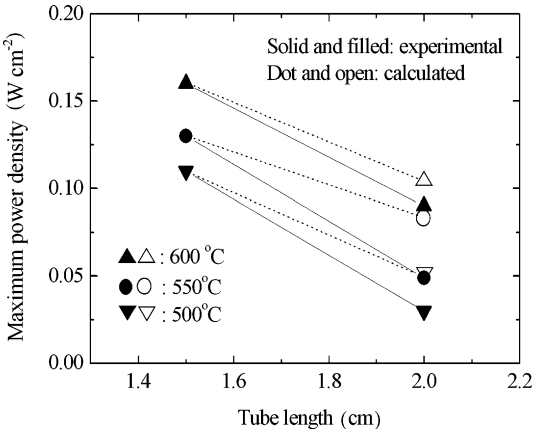

Fig. 14. Maximum power densities of the cells as a function of tube length.

the porous cathode with the well-dispersed Ag particles to obtain an obviously improved conductivity [23]. It is also feasible to design a small interconnect, as discussed previously by Ota et al. [24]. On the other hand, a concept using the cube-shaped cell bundle [25], where the cells are integrated in a metal (Ni) matrix, can possibly make these cathode-supported micro-tubular cells towards application with a high volumetric power density.

4. Conclusion

A dense thin $Ce_{0.9}Gd_{0.1}O_{1.95}$ electrolyte (thickness < 15 μm) and a Ni–cermet anode (Ni:$Ce_{0.9}Gd_{0.1}O_{1.95}$ = 50:50 in volume after reduction, thickness < 10 μm) on a porous $La_{0.6}Sr_{0.4}Co_{0.2}Fe_{0.8}O_{3-\delta}$/$Ce_{0.9}Gd_{0.1}O_{1.95}$ (60:40 in volume) cathode tube have been successfully fabricated by a cost-effective technique involving extrusion molding and slurry coating through a co-firing process. Co-firing temperatures for cathode/electrolyte and subsequent anode formation were 1200 and 1100 °C, respectively. The wall thickness and diameter of the cells were 460 (m and 2.26 mm. The micro-tubular cathode-supported cell with 1.5 cm long tube yielded maximum power densities of 0.16, 0.13 and 0.11 W cm^{-2}, at 600, 550 and 500 °C, respectively. The analysis revealed that the present current collection way for the cathode tube during single cell measurement, as well as the relatively low-open circuit voltage due to the current leakage of the ceria electrolyte influenced by the support electrodes and the fabrications, highly hinder the cell performance.

Acknowledgement

This work has been supported by NEDO, Japan, as part of the Advanced Ceramic Reactor Project.

References

[1] B.C.H. Steel, Solid State Ionics 75 (1995) 157.
[2] O. Yamamoto, Y. Arati, Y. Takeda, N. Imanishi, Y. Mizutani, M. Kawai, Y. Nakamura, Solid State Ionics 79 (1995) 137.
[3] T. Ishihara, H. Matsuda, Y. Takita, J. Am. Chem. Soc. 116 (1994) 3801.
[4] L.W. Tai, M.M. Nasrallah, H.U. Anderson, D.M. Sparlin, S.R. Sehlin, Solid State Ionics 75 (1995) 273;
L.W. Tai, et al., Solid State Ionics 76 (1995) 259.
[5] Z. Shao, S.M. Haile, Nature 431 (2004) 170.
[6] S.J. Skinner, J.A. Kilner, Solid State Ionics 135 (2000) 709.
[7] M. Williams, in: H. Yokogawa, S.C. Shinghal (Eds.), Solid Oxide Fuel Cells VII, PV 2001-16, The Electrochemical Society Proceedings Series, Pennington, NJ, 2001, p. 3.
[8] I.P. Kilbride, J. Power Sources 61 (1996) 167.
[9] K. Kendall, M. Palin, J. Power Sources 71 (1998) 268.
[10] N.M. Sammes, Y. Du, R. Bove, J. Power Sources 145 (2005) 428.
[11] T. Suzuki, T. Yamaguchi, Y. Fujishiro, M. Awano, J. Electrochem. Soc. 153 (2006) A925.
[12] Y. Liu, S. Hashimoto, H. Nishino, K. Takei, M. Mori, J. Power Sources 164 (2007) 56.
[13] K. Yamahara, C.P. Jacobson, S.J. Visco, L.C. De Jonghe, Solid State Ionics 176 (2005) 451.
[14] H. Ohrui, T. Matsushima, T. Hirai, J. Power Sources 71 (1998) 185.
[15] E. Suda, B. Pacaud, Y. Montardi, M. Mori, M. Ozawa, Y. Takeda, Electrochemistry 71 (2003) 866.
[16] M. Sasaki, Ceram. Jpn. 32 (1997) 812.
[17] V. Dusastre, J.A. Kiliner, Solid State Ionics 126 (1999) 163.
[18] J.W. Moon, H.W. Lee, H.G. Kang, J.D. Kim, G.D. Kim, H.L. Lee, in: M. Dokiya, O. Yamamoto, H. Tagawa, S.C. Shinghal (Eds.), Solid Oxide Fuel Cells IV, PV 2001-16, The Electrochemical Society Proceedings Series, Pennington, NJ, 1995, p. 282.
[19] D. Waldbillig, A. Wood And, D.G. Ivey, Solid State Ionics 176 (2005) 847.
[20] K. Huang, J. Electrochem. Soc. 151 (2004) A716.
[21] D.P. Fagg, V.V. Kharton, J. Frade, J. Electroceram. 9 (2002) 199.
[22] T. Suzuki, T. Yamaguchi, Y. Fujishiro, M. Awano, J. Power Sources 163 (2007) 737.
[23] Y. Liu, M. Mori, Y. Funahashi, Y. Fujishiro, A. Hirano, Y. Takeda, The 15th Symposium on Solid Oxide Fuel Cells in Japan, Tokyo, Japan, 2006, p. 112.
[24] T. Ota, M. Koyama, C. Wen, J. Power Sources 118 (2002) 430.
[25] Y. Funahashi, T. Shimamori, T. Zusuki, Y. Fujishiro, M. Awano, J. Power Sources 163 (2007) 731.